Relevance of Wavelet Shape Selection in a complex signal

Maxence Bigerelle, Gildas Guillemot, Zahra Khawaja, Mohamed El Mansori, Jérôme Antoni

Relevance of Wavelet Shape Selection in a complex signal

M. Bigerelle [a,b,*], G. Guillemot [c,1], Z. Khawaja [d,2], M. El Mansori [e,3], J. Antoni [f,4]

[a] Laboratory For Automation Mechanical Engineering Information Sciences and Human-Machine Systems, UMR CNRS 8530, Le Mont Houy, 59313 Valenciennes, France
[b] Laboratory of Thermics, Energetics, Mechanics, Process and Production, Université de Valenciennes et du Hainaut Cambrésis, Le Mont Houy, 59313 Valenciennes, France
[c] CEMEF, Centre de Mise en Forme des Matériaux, MINES ParisTech, Rue Claude Daunesse, BP 207, 06904 Sophia Antipolis, France
[d] Laboratoire Roberval, UMR 6253, UTC/CNRS, Centre de recherche de Royallieu, BP 20259, 60205 Compiègne, France
[e] Arts et Métiers ParisTech, Mécasurf, 2 cours des Arts et Métiers, F-13617 Aix en Provence, France
[f] Laboratory Vibrations Acoustics LVA, University of Lyon, F-69621, 25 bis avenue Jean Capelle, 69621 Villeurbanne, France

Keywords:
Wavelet
Discrete wavelets transform
Multiscale analysis
Variance analysis
Roughness

A B S T R A C T

In wavelet analysis, the signal reconstruction and statistical estimators are strongly influenced by the wavelet shape that controls the time-frequency localization properties. However, this dependency does not imply that the wavelet form is physically relevant to extract spatially invariant wavelet-based shape signatures. A new statistical estimator is proposed in order to quantify the influence of the wavelet on the spatial detection. This indicator is then used to analyze signals obtained from the topography of abraded surfaces. It is shown that the Coiflet wavelet is physically adapted to reproduce the elementary mechanical process which creates the abrasion of the surface. Using 8 different wavelets, the analysis of the signal obtained by scanning the abraded surface leads to the same spatial localization regardless the parameters of the abrasive process and whatever the wavelet shapes. No statistical difference related to the type of wavelets is found between the indicators (RMS, spectral moments…) extracted from the reconstructed signals calculated on different scales and for various abrasive processes. If the wavelet decomposition is seen as a multiscale microscope, a surface can be seen in different ways according to the type of wavelets. However, the morphological changes of the surface caused by external mechanical causes and characterized by several statistical parameters are statistically similar regardless the shape of the wavelets.

1. Introduction

Precision machining by turning and rectifying of functional surfaces of mechanical parts, i.e. obtaining flawless parts both on the geometrical and structural aspects requires a considerable technical and economical effort. Some operations are

* Corresponding author at: Laboratory For Automation Mechanical Engineering Information Sciences, Human-Machine Systems, UMR CNRS 8530, Le Mont Houy, 59313 Valenciennes, France. Tel.: +33 3 27 51 19 77; fax: +33 3 27 51 19 61.
E-mail addresses: Maxence.Bigerelle@univ-valenciennes.fr, maxence.bigerelle@utc.fr (M. Bigerelle), gildas.guillemot@mines-paristech.fr (G. Guillemot), Zahra.khawaja@utc.fr (Z. Khawaja), mohamed.elmansori@ensam.eu (M. El Mansori), jerome.antoni@insa-lyon.fr (J. Antoni).
[1] Tel.: +33 4 93 67 89 27; fax: +33 4 92 38 97 52.
[2] Tel.: +33 3 44 23 44 23x48 91; fax: +33 3 44 23 49 84.
[3] Tel.: +33 4 42 93 82 64; fax: +33 3 26 69 91 97.
[4] Tel.: +33 4 72 43 71 83; fax: +33 4 72 43 87 12.

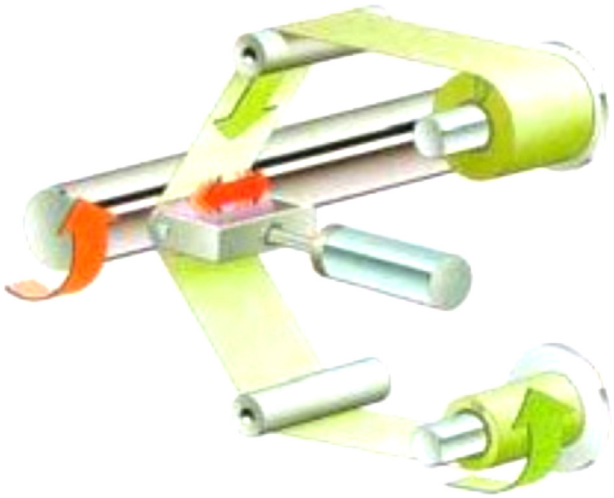

Fig. 1. The grinding belt principle [1].

completed by a finishing process such as the belt grinding process (Fig. 1) which is easier and less expensive than others finishing processes like high precision tool machining. However, we still have an incomplete knowledge of both the mechanisms and the characteristics of this process. Some authors analyzed the relations between the conditions of this process and the roughness of the obtained surfaces by experimental approaches [1,2].

A surface generated by machining is composed of a large number of irregularities (peaks and valleys) superimposed on more widely spaced undulations (waviness). These irregularities, known as roughness, are generally characterized by three types of parameters: amplitude parameters, spatial parameters, and hybrid parameters (see Table 1). Amplitude parameters measure the vertical heights of the surface deviations from a reference line. Spacing parameters measure the horizontal characteristics of the surface deviations. Hybrid parameters are a combination of both the vertical and the horizontal characteristics of surface deviations.

It should also be noticed that the abrasion process is stochastic since the mechanical properties, the movement, and geometrical properties of the cutting tips are all characterized by a large statistical variability. For example, Pellegrin et al. model abrasion with a Monte Carlo approach [3]. In the same way, Bigerelle et al. [4,5] prove that abraded surfaces can be modeled by stochastic fractal functions and using the Monte Carlo model, and thus the belt finishing process as well [6]. This stochastic aspect is also used to take into account the roughness in the abrasion model thanks to the Gaussian approximation of surface roughness [7]. Simple sclerometric rheological material analysis shows geometrical dependences of ridge height and groove depth, in combination with the Peaks and Valleys (PV) [8]. In fact, Peaks and Valleys (PV) of roughness are linked to abrasion. King et al. link the resistance of optical coatings to scratching to PV [9]. The transient behavior of super-finished surfaces has been examined by Malkin and co-workers [10,11]. They found that the radial stock removal during the transient stage is approximately equal to the average PV of the initial ground surface. Chang et al. [12] have used the PV amplitude to investigate the effect of process parameters on the evolution of the texture of super-finished surfaces obtained by stone super-finishing of hardened AISI 8119 steel. Experimental results suggest a linear correlation between SSD (Sub Surface Damage) depth and PV with a proportionality constant for various materials Glass [13,14]. This linear relation was explained and modeled by Miller et al. [15] by applying micro-indentation mechanics and built models for the SSD/surface roughness ratio based on the indentation of sharp and spherical indenters, with respect to material mechanical properties, shape and load of abrasive grains. In fact, the use of the PV is justified by a model proposed by Jha and Jain [16] based on the local erosion of peaks.

However, the stochastic aspect of abrasion leads to local accumulation of damages resulting in highest peaks or deepest valleys and their amplitudes depend on the scale of observation. It is shown that abraded surfaces possess a fractal structure [17] that was naturally found on wear debris [18] and can be used for wear prediction [19]. However, the fractal concept cannot be applied to all the scales and an upper scale is often found from which it fails. This bi-structure was first introduced by Bhushan et al. [20] to propose an elastic–plastic contact model of a magnetic tape in contact with a flat hard plane. Wu also used the bi-fractal formalism to model abrasion [21]. This approach yields two fractal functions defined on two bandwidths. This means that the second stage follows also a fractal structure and finally abrasion is a superposition of fractal structures with two distinct scaling laws. In fact, a high number of bi-fractal structures met in the bibliography are based on a visual observation of a graph called the “log–log plot” (plot of a mathematical measure versus the scale of observation in logarithmic coordinates) of which the slope is related to the fractal dimension: if a cross over appears in the log–log plot, then a bi-fractal structure is shown. However, it has been also proved that a log–log plot obtained from abraded surfaces can present a bi-fractal structure without having a scaling law for the highest scale and can only be due to a severe cumulation

Table 1
2D roughness parameters used to quantify the roughness of profiles (from Whitehouse, DJ, 2003, Handbook of Surface Nanometrology, IOP Publishing, Ltd., London).

Parameter name	Definition	Classification
R_p	Maximum profile peak height within a sampling length	Amplitude parameters
R_v	Maximum profile valley depth within a sampling length	
R_z	Maximum height of the profile within a sampling length	
$R_{v1}\ldots R_{v5}$	Maximum local profile valleys height	
$R_{p1}\ldots R_{p5}$	Maximum local profile peak height	
$R_{z1}\ldots R_{z5}$	Maximum local height of the profile	
R_{z3}	Mean local height of the profile	
R_{wz}	Mean local curvature radii of peaks	
R_c	Mean height of the elements of the profile, inside a sampling length	
R_t	Total height of the profile on the evaluation length	
R_a	Arithmetic mean deviation of the assessed profile	
R_q	Root-Mean-Square (RMS) deviation of the assessed profile	
R_{sk}	Skewness (asymmetry) of the assessed profile	
R_{ku}	Kurtosis of the assessed profile	
R_{mr}	Relative material ratio	
R_{dc}	Profile section height difference (bearing height)	Material ratio parameters
R_{Sm}	Mean width of profile elements, within a sampling length	Spacing parameters
R_{dq}	Root-Mean-Square (RMS) slope of the profile within a sampling length	
R_k	Kernel roughness depth (roughness depth of the core)	Parameters based on the linear material ratio curve
R_{pk}	Reduced peak height (roughness depth of the peaks)	
R_{vk}	Reduced valley depth (roughness depth of the valleys)	
M_{R1}	Upper material ratio	
M_{R2}	Lower material ratio	
A_1	Upper area (area of the triangle equivalent to the peaks)	
A_2	Lower area (area of the triangle equivalent to the holes)	
R^*_{pk}	Peak height (roughness depth of the peaks, before area correction)	
R^*_{vk}	Valley depth (roughness depth of the valleys, before area correction)	
R_{pq}	Plateau Root-Mean-Square (RMS) roughness of the profile	Parameters based on the material probability curve
R_{vq}	Valley Root-Mean-Square (RMS) roughness of the profile	
R_{mq}	Material ratio at plateau-to-valley transition of the profile	
R	Mean depth of the roughness motifs	Parameters linked to the roughness motifs
A_R	Mean spacing of the roughness motifs	
R_x	Maximum depth of the roughness motifs	
P_t	Total height of the profile	
K_r	Mean slope of the roughness motifs	
N_r	Number of roughness motifs	
S_R	Standard deviation of the depth of the roughness motifs	
S_{AR}	Standard deviation of the spacing of the roughness motifs	
T_{rc}	Microgeometric material ratio	Bearing ratio at a given depth
H_{Trc}	Microgeometric criterium (height between two bearing ratios)	
R_{ke}	Kernel roughness of the envelope-leveled profile	
R_{pke}	Reduced height of the envelope-leveled profile	
R_{vke}	Reduced depth of the envelope-leveled profile	
R_t	Total Height of roughness profile	
R_{pm}	Average maximum profile peak height of the roughness profile	ASME B46.1 parameters
$R\Delta_a$	Arithmetic mean slope on the roughness profile	
W_t	Total height of waviness profile	
Δ_v	Variation method	Fractal dimensions
Δ_s	Structure method	
Δ_a	AMN method	
Δ_b	Box counting method	
Δ_d	Dilatation method (Bouligand)	

of damages whose probability of occurrence naturally increases with the scale of observation without presenting a scaling correlation, i.e. fractal behavior.

Wavelet theory has become an active area of research in many fields such as sound synthesis, vibration/motion analysis, transient signal analysis, data smoothing/de-noising, image compression, communication systems, feature extraction, subband coding, and other signal processing applications. In this paper, a multiscale analysis using the discrete wavelet transform is performed on the measured signals in order to find the relations between the finishing process and the roughness of the surface. The objective of this paper is to determine the effect of the choice of the mother wavelet on the results of the analysis. The aim is to identify the most relevant roughness parameter and its characteristic length in order to assess the influence of finishing process, and to test the relevance of the measurement scale.

2. Experimental study

The grinding belt process (Fig. 1) consists in applying an abrasive oscillating belt, of low thickness, on a rotating manufactured specimen. To assure the reproducibility of the process, five inner parts of ball bearing designed as100Cr6 steel grade, having a diameter of 54.78 mm and a width of 30 mm, are tooled (ie. superfinished by process) for each group of test conditions of the experimental design. The width of the belt is 20 mm. Tagushi's experimental design is used to study the effects of the belt grinding process conditions on the resulting roughness. The experiment is conducted using 16 specimens that were turned and rectified. The initial roughness parameters are *Rz*, 18.3 μm; *Rmax*, 20.1 μm; *Ar*, 134 μm; *War*, 1050 μm; *Wr*, 8 μm; *RPk*, 8.1 μm; *Rk*, 15.4 μm; *Rvk*, 7.8 μm. All samples are then manufactured with the same lubrication condition corresponding to reference 'Cut Max H05'. We retain 7 process parameters: Belt feed (50 and 100 mm/mn), contact pressure (1 and 3 bar), Axial oscillation frequency (1.6 and 10 Hz), contact wheel stiffness (hard and soft), cycle times (3 and 9 s), belt grit size (9 and 40 μm) and finally work piece rotation speed (100 and 500 rpm) [22].

This experimental design is built to take into account the interactions between the contact wheel stiffness, the contact pressure, and the belt grit size. Roughness measurements are performed for each specimen. For each measurement, 30 roughness signals were recorded from the tooled surfaces by a KLA-TENCOR™ P-10 profilometer with a 2 μm tip radius. The scanning and the sampling lengths are, respectively, 8 mm and 0.1 μm. The real resolution on our samples is analyzed in Appendix A and can be estimated to 1 μm in lateral direction. Under this critical length, signal analyses cannot be formally performed because of a smoothing effect due to tip radius.

3. Multiscale problem statement of abrasion

In this part, the multiscale aspect of abrasion will be described precisely to justify the use of the wavelet analysis to characterize the different physical parameters of the abrasion mechanisms. Abrasive processes work by forcing the abrasive particles, or grains, into the surface of the workpiece so that each particle cuts away and simultaneously deforms in visco-elasto-plastic or brittle manner a small volume of material. This process can be divided into two categories based on how the grits are applied to the work piece. In the first category, bonded abrasive processes, called "two body abrasion", the particles are held together within a matrix, and their combined shape and density determine the geometry and morphology of the finished work piece. In the second category, loose abrasive processes, called "three body abrasion" there is no firm structure bounding the grains The common "two body abrasion" bonded abrasive processes are wheel grinding, stone honing, belt or tape finishing, buffing, brushing, grains wire cutting or sawing, etc. Largely known "three body abrasion" or loose abrasive processes are polishing, lapping, abrasive flow or jet machining, blasting and in mass finishing.

3.1. Study of elementary abrasion processes

During the "two-body abrasion", when hard abrasives usually simultaneously remove and deform ductile material by "micro-cutting", plastic deformation of abraded material occurs. To quantify individually the effect of an isolated abrasive grain, a sclerometer is used to measure the scratch hardness of materials. The sclerometer test consists of microscopically measuring the width of a scratch made by a diamond under a fixed load, and drawn across the face of the specimen under fixed conditions. Fig. 2 schematically shows a cross section of a groove created by the sclerometer with ridges. Considering a cross section the loss caused by a single grit can be determined [23,24] by $\beta = 1 - (A_b + A_{b'})/A_v$ where A_b, $A_{b'}$ and A_v, respectively, represent the volume of material displaced on the left hand side and on the right hand side of the scratch, and the volume of the scratch above the mean line (Fig. 2). It has been known that wear rate of materials is closely related to the grit size in "two-body abrasion" in relationship with the dimensions of the scratch profile. Nevertheless, a plastic deformation behavior of abraded material still has a strong effect on the wear process [25]. It can be inferred that the critical particle size effect can be explained directly from β factor because it shows the true fraction of cutting wear among the grooving materials. However, the exact measurement of ridge geometrical parameters is difficult and tedious after scratching. Thus, the implementation of computer simulation is desirable. It is interesting to note that Bucaille et al. [26] simulated an indenter scratching process on elastic–plastic plate using Forge3® and a regressive expression was proposed that builds a relationship between the shape ratio and rheological factor which is in agreement with the experimental results of Jardret et al. [24], and Mathia et al. [27].

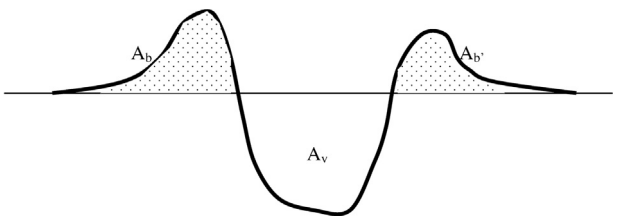

Fig. 2. Transversal scanning of a groove.

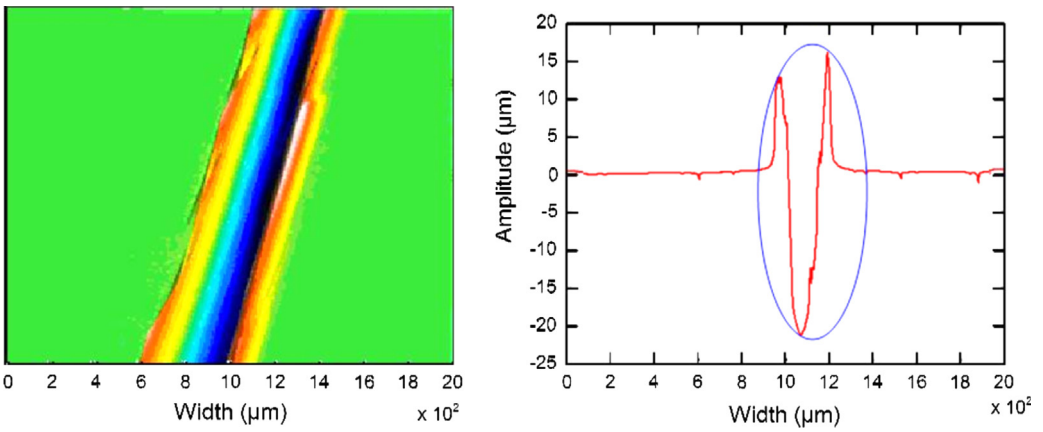

Fig 3. (a) A surface with one deep scratch. (b) The '*V*' form of a scratch.

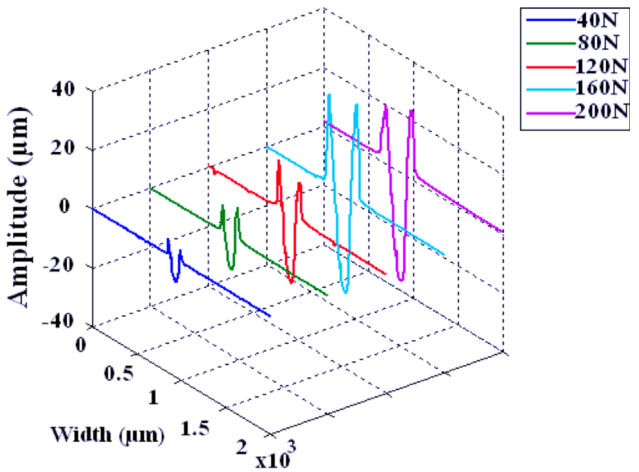

Fig. 4. Various scratch signals resulting from applying different forces. The amplitude of the signal increases with the value of applied force (in Newton).

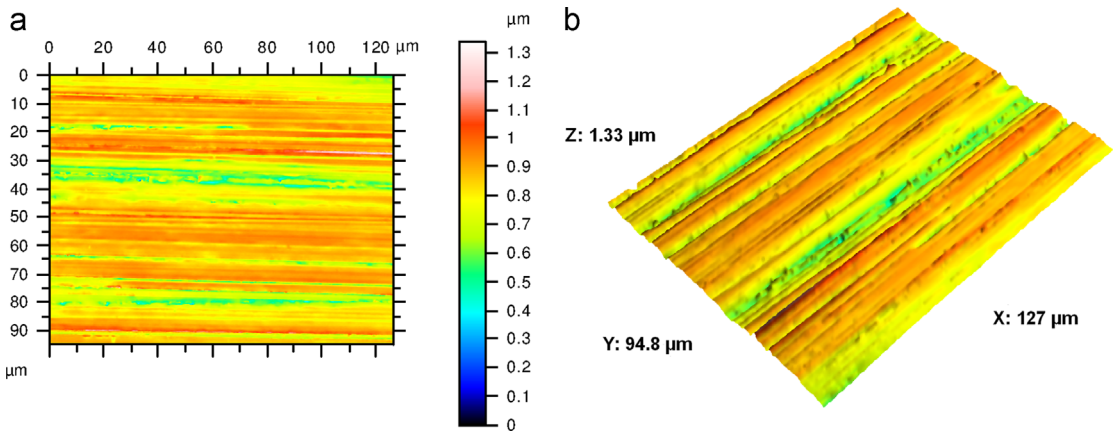

Fig. 5. A signal obtained by microscope interferometric scanning on an abraded surface (640∗480 sampling data).

A sclerometer test (also called "scratch test") is performed on the retained materials that model physically the scratches produced by the abrasive grains of the grinding belt. Fig. 3 represents the three dimensional scratches recorded by a 3D profilometer. As shown in Fig. 2, the scratch is identified as a "*V*" shape in the signal obtained by the profilometer when scanning an abraded surface (see Fig. 3). The amplitude of the groove depends on the force applied on the indentor of the scratch test: Different loads are applied (40–200 N) and grooves are recorded: the higher the load, the deeper the groove on

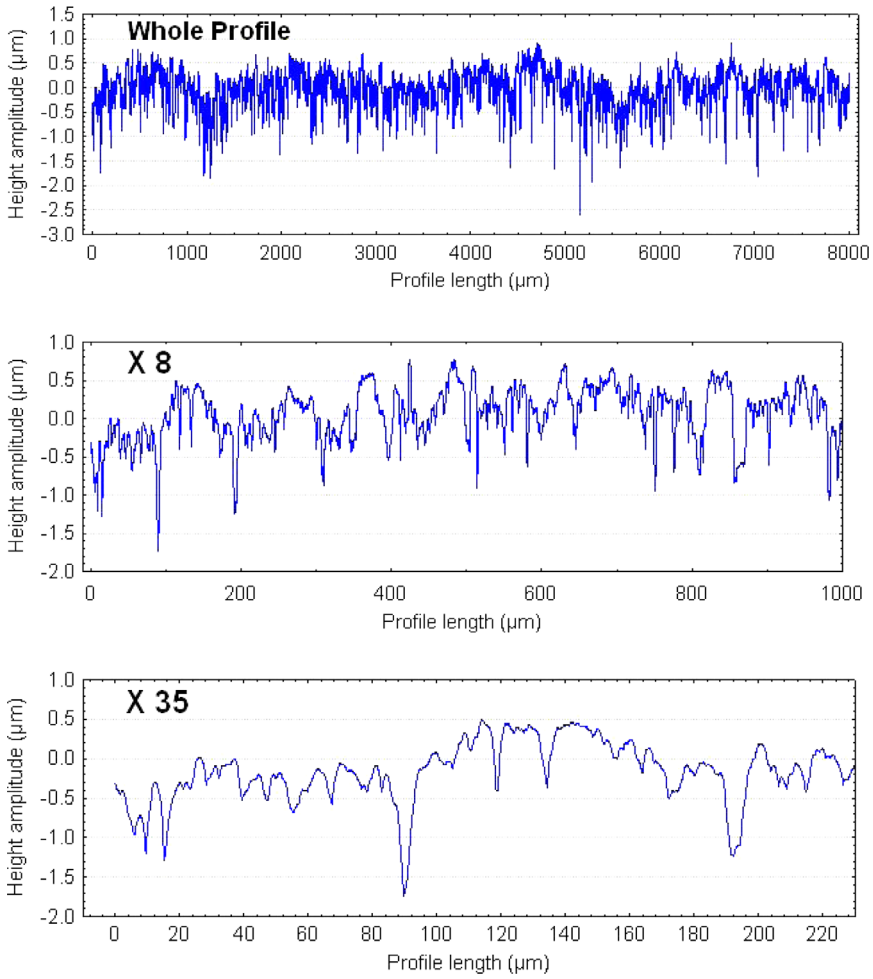

Fig. 6. A signal obtained by scanning mechanically an abraded surface tooled by the belt finishing process (120,000 sampling data) from Bigerelle et al. in [27].

the surface (Fig. 4). For example, by applying a force of 200 N the amplitude of the scratch is between -40 µm and $+30$ µm, whereas for a force of 40 N the amplitude is between -7 µm and $+5$ µm.

Fig. 5 represents the surface topography of an abraded surface scanned by Interferometry (640∗480 sampling data). To appreciate the multiscale aspect of abrasion, the surface is recorded by a high resolution stylus profilometer (150,000 sampling data) and different zooms are performed (Fig. 6).

Wavelets are often used to analyze the multiscale aspect and particularly the fractal aspect of the abrasion [28–30]. As a consequence, one could postulate that a wavelet that well models the elementary process of the scratch test could be more relevant to characterize accurately the different scales of abrasion induced by each parameter of the Belt Finishing Process.

4. Wavelet analysis of signal

4.1. Objective of the wavelet decomposition

From a tribological point of view, our purpose is to find how the level of the retained process parameters (see Table 2) modifies the surface roughness. More precisely, at which scale range, each process parameter affects the morphology of the surface. Initially, the different shapes of the wavelets used to analyze the multiscale aspect of the signals will be presented. In this paper, only discrete wavelets will be used. To analyze the effect of wavelet shape on the signal characterization, different wavelet shapes are retained. Particularly, different Debauchies' wavelets will be used (with orders: 2, 5, 8, 10) that introduce various shapes due to an increase of wavelet oscillation and regularity with the order. Then the relevance of characterizing the form of the elementary signal (i.e. the scratch, Fig. 3) by all retained wavelets is analyzed and quantified. Then, the 3 different scale decompositions corresponding to high frequencies, low frequencies and details (signal at a fixed

Table 2
Description of the Tagushi experimental design.

Experiment	Contact wheel stiffness	Belt grit size (μm)	Contact pressure (bar)	Workpiece rotation speed (rpm)	Belt feed (mm/mn)	Cycle time (s)	Axial oscillation frequency (Hz)
1	Hard	9	1	100	50	3	1.6
2	Hard	9	1	500	100	9	10
3	Hard	9	3	100	50	9	10
4	Hard	9	3	500	100	3	1.6
5	Hard	40	1	100	100	3	10
6	Hard	40	1	500	50	9	1.6
7	Hard	40	3	100	100	9	1.6
8	Hard	40	3	500	50	3	10
9	Soft	9	1	100	50	3	10
10	Soft	9	1	500	100	9	1.6
11	Soft	9	3	100	50	9	1.6
12	Soft	9	3	500	100	3	10
13	Soft	40	1	100	100	3	1.6
14	Soft	40	1	500	50	9	10
15	Soft	40	3	100	100	9	10
16	Soft	40	3	500	50	3	1.6

scale) are applied on signal roughness. As is usually the practice in the topics of surface metrology, roughness parameters are computed on these signals.

4.2. Most relevant wavelet to characterize the elementary mechanism of abrasion

For the last decade, they have been used in roughness analysis to filter the signal. In the present study, 8 different discrete mother wavelets are considered (Debauchies 2,5,8,10, Coiflets, Symlets, Meyer, and Biorthogonal). Various authors report that the choice of a wavelet shape is the most important step in wavelet analysis, because it guarantees a precise decomposition of the original signal into different frequency resolutions [38–44]. The criteria used to choose the mother wavelet that is best suited to the signal depend strongly on the studied physical process. The most successful is the one using the mother wavelet that best matches the shape of the analyzed signal [31–33]. The abraded surface is composed of a succession of individual scratches due to indentation of grits. Pressure is different for each grit in the rubber and as a consequence scratches will be more or less deep. It would be suitable to think that the morphology of an abraded surface (see Fig. 6) will be accurately decomposed by the wavelet transform if the shape of the wavelet well fits the topography of an individual scratch (see Figs. 3 and 4). To quantify the relevance of the wavelet shape, an optimization algorithm is constructed to find the best amplitude, scaling and translation that fits all the experimental topographies of individual scratches (Fig. 8).

A statistical analysis shows that the mother wavelet of “Coiflet” (see Fig. 7d) is the most suited to identify an individual scratch (lower amplitude of the residuals between the wavelet and the topography of the groove) because its scaling function matches the transient shape of the scratch (Figs. 3 and 4). Fig. 7 shows the others different wavelets used to fit the individual scratch. A precise analysis is performed in Appendix B.

4.3. Multiscale decomposition

The surface geometrical structure in its longitudinal and lateral profiles contains complex characteristics of surface irregularities with roughness, waviness and shape components along the measured length. In the tool processing technology, turning, milling, grinding and all other machining processes impose characteristic irregularities on a part of the surface. Additional factors such as cutting tool selection, machine tool condition, speeds, feeds, vibration and other environmental influences further influence these irregularities. On analysis, texture can be broken down into three components: roughness, waviness, and form. Roughness is essentially synonymous with tool marks. Every pass of a grit of the abrasive paper leaves a groove of some width and depth. Errors of form are due to a lack of straightness or flatness in the ways of the machine tool or due to the fact that the part is not nominally straight and/or flat (cylinder, sphere…). This is a highly repeatable type of irregularity, as the machine will always follow the same out-of-straight path and can be removed by regression with an appropriate functional that describes the form (a three order polynomial function is often well relevant).

Then the engineering surfaces considered here consist of a range of spatial frequencies. The high frequency or short wavelength components are referred to as roughness and the medium frequency components as waviness. Applying wavelet analysis, parts produced by abrasion (roughness) may be defined as any irregularity with wavelet width shorter than W (μm); waviness greater than W. According to these remarks, Three types of multiscale decomposition will be proposed to characterize the topography: (1) the roughness is analyzed by the lower wavelet width summation defined as the B decomposition) and (2) the waviness is analyzed by the higher lower wavelet width summation defined as the A decomposition. (3) The classical D decomposition (Details) corresponding to a given decomposition with a unique wavelet

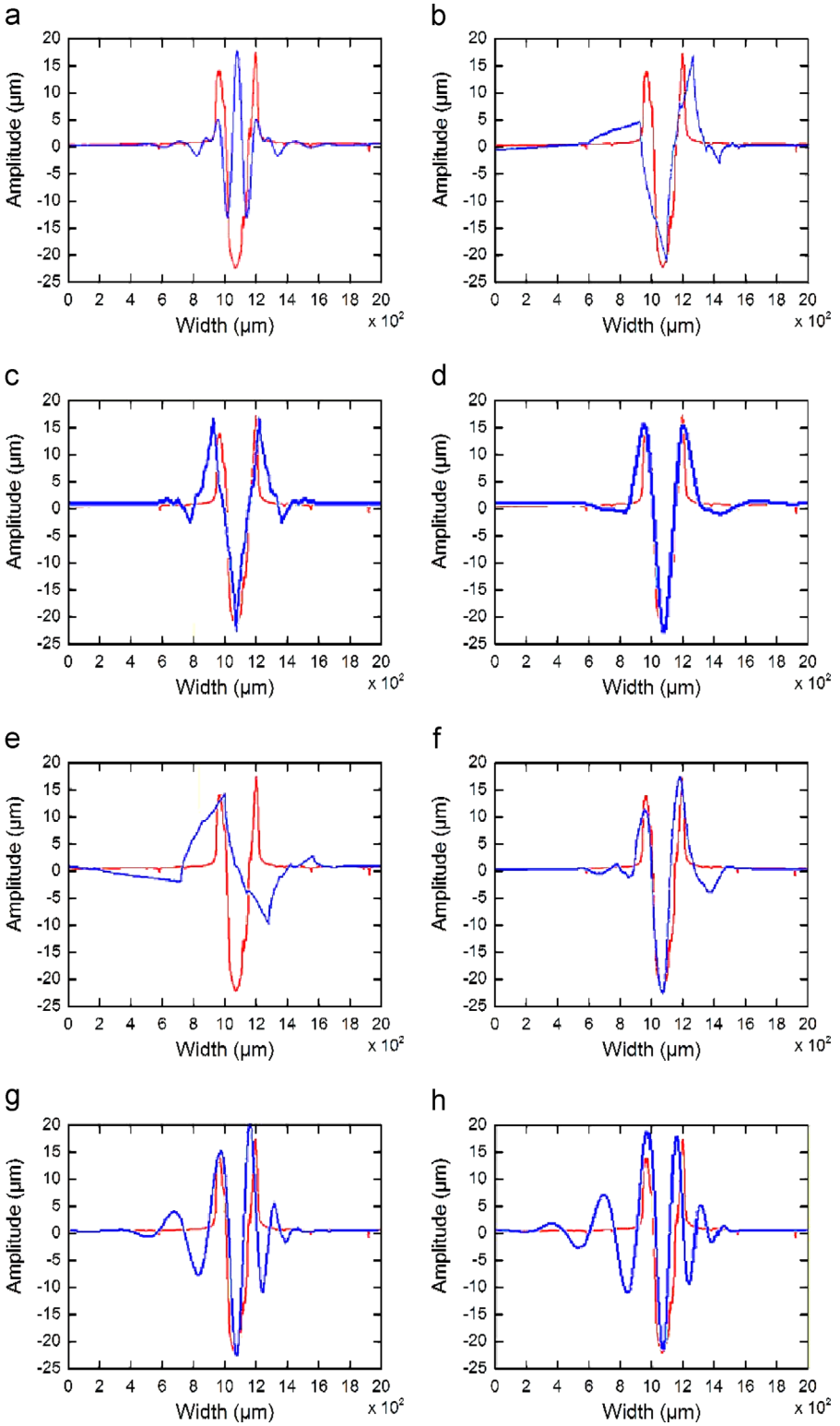

Fig. 7. Representation of the scratch signal (red) and the used wavelets (blue). (a) Meyer wavelet, (b) Symlet wavelet, (c) Biorthogonal wavelet, (d) Coiflet "3", (e) Daubechies "2" wavelet, (f) Daubechies "5" wavelet, (g) Daubechies "8" wavelet and (h) Daubechies "10" wavelet. (For interpretation of the references to color in this figure caption, the reader is referred to the web version of this article.)

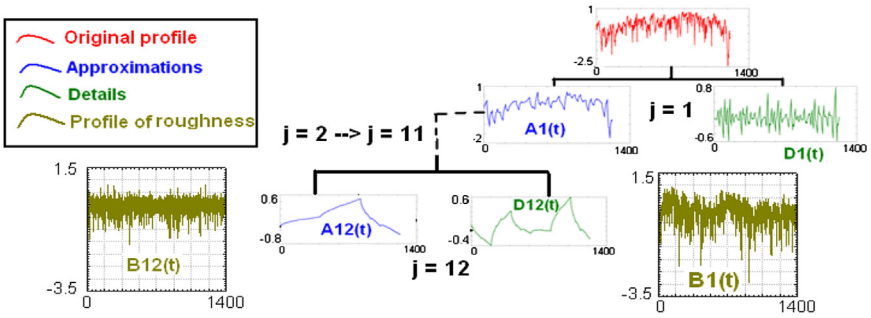

Fig. 8. An example of the three decompositions (A, B, and D) for two levels, $j=1$ and $j=12$.

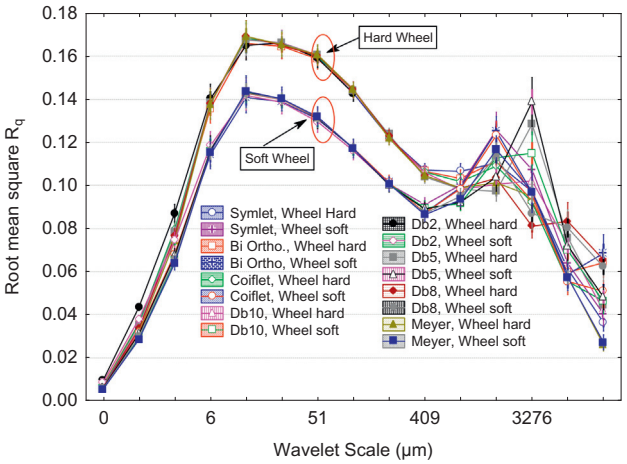

Fig. 9. Evolution of the root mean square versus the evaluation length for the two levels of contact wheel stiffness with different wavelets shapes obtained by the detail decomposition D.

width will also be considered. Fig. 8 displays the wavelet decomposition of an initial signal of the topography of the surface. To evaluate the scale of decomposition ε, the following relations will be stated: let M be the number of decompositions ($M=17$ in our case), j the order of the wavelet decomposition and dt the sampling length, then for the B decomposition one gets $\varepsilon = dt\ 2^{M-j+1}$ and for A and D $\varepsilon = dt\ 2^{j}$

4.4. Roughness parameters

Because of these various industrial and scientific interests, a proliferation of roughness parameters, possibly running into hundreds, has been triggered to describe the different kinds of surface morphology with regard to specific functions, properties, or applications. In an industrial environment and in research laboratories, it is common to quantify surface morphology in terms of roughness parameters in terms of amplitude (the arithmetic average roughness R_a, root-mean square roughness RMS (R_q), frequency (peak-to-valley roughness R_t or number of peaks per inch N_p, autocorrelation length…) and hybrid (slope of profile, surface ratio). Such roughness parameters are estimated to qualify the surface quality of the products (see Table 1 for the exhaustive list of parameters used in this study).

4.5. Multiscale analysis of roughness parameter

As described in Section 4.4, each profile is decomposed in successive multiscale series of three profiles (High frequency (B), Low frequency (A), and Details (D)) from which roughness parameters can be computed. The following notation is adopted, where $q_i(\varepsilon, w, d, K, n)$ represents the roughness parameter q_i computed from the n-th profile taking in K process conditions and transformed by a decomposition d with a wavelet shape w of width ε. The evolution of the root mean square roughness parameter versus the scale taking account the contact stiffness of the wheel (soft, hard) for different wavelet shapes used in the D decomposition is given in Fig. 9.

Without introducing mathematical concepts, it can be quickly observed that:

- The root mean square depends on the scale.
- A difference exists between the hard steel wheel and the soft wheel.

- The choice of wavelet shape seems to affect slightly the value of these roughness parameters at all the scales.
- Two maxima of R_q values are located at two characteristic lengths. The first one corresponds to a value close to 18 μm. The second one is less defined and corresponds to a value of the order of 2–3 mm. This value is less relevant. Indeed this characteristic length is greater than 20% of the surface analyzed length. New measurements should be conducted on greater lengths to conclude on its relevance and to have a precise estimation of its value.

5. Relevance of multiscale decomposition

The main problem is to answer the following questions:

- How to select the most relevant scale giving the highest roughness difference between groups of specimens tooled with the two contact wheel stiffness?
- Which roughness parameter better quantifies this difference if the latter is significant?
- Does this difference depend on the shape of the wavelet used to perform the decomposition?
- What is the most relevant method of filtering (high, detail or low frequency signals)?

A statistical method will be used to answer these questions.

5.1. Analysis of variance with bootstrap resampling

The most relevant scale is investigated by the analysis of variance which is an implementation of the generalized linear model. The formalism is defined as follows:

Let

$$q_i(\varepsilon, w, d, k_1, k_2, \ldots, k_p, n) = \alpha_0(i, w, d, \varepsilon) + \sum_{j=1}^{p} \alpha_{j,k_j}(i, w, d, \varepsilon) + \sum_{j=1}^{p} \sum_{l=j+1}^{p} \beta_{j,k_j,l,k_l}(i, w, d, \varepsilon) + \xi_{k_1,k_2,\ldots,k_p,n}(i, w, d, \varepsilon) \quad (1)$$

where $q_i(\varepsilon, w, d, k_1, k_2, \ldots, k_p, n)$ is the roughness parameter (indexed by i) of the n-th profile when the p process parameters are taken at levels $k_1, k_2, \ldots, k_p$, for an ε scale decomposition with a filtering d computed with a wavelet w, $\alpha_{j,k_j}(i, w, d, \varepsilon)$ is the influence on the roughness parameter value of the j-th process parameter at k_j level, $\beta_{j,k_j,l,k_l}(i, w, d, \varepsilon)$ is the influence of the interaction between both k_j and k_l process parameters, and $\xi_{k_1,k_2,\cdots,k_p,n}(i, w, d, \varepsilon)$ is a Gaussian noise with zero mean and σ standard deviation.

For each wavelet w, each of the three types of filter d and each scale ε, all of these influences are calculated by analysis of variance. From them and for each process parameter k_j and each interaction, between-group variability and within-group variability (corresponding to errors of estimation of the roughness parameter into each group) are calculated. The result denoted as $F(q_i, w, d, \varepsilon, k_j)$ is the ratio produced by dividing the between-group variability by the within-group variability. In other words, this result compares the effect of each process parameter on the roughness parameter value with its estimation error. Consequently, for a given process parameter, a value of the Fisher Criterion $F(q_i, w, d, \varepsilon, k_j)$ near 1 translates an irrelevancy of the roughness parameterq_i estimated at the evaluation length ε to represent effects of the considered process parameter. The higher the $F(q_i, w, d, \varepsilon, k_j)$ value, the more relevant the parameter $q_i$estimated at scaleε is (see [22] for more details). The highest $F(q_i, w, d, \varepsilon, k_j)$ value allows selection of the most pertinent roughness parameter and its evaluation length to describe the influence of the given process parameter. Then a bootstrap protocol developed by the authors is applied to quantify variability on the $F(q_i, w, d, \varepsilon, k_j)$ value [29].

5.2. Multiscale graph of relevance

Next the value of $F(q_i, w, d, \varepsilon, k_j)$ can be plotted versus the scale for the roughness parameter q_i characterizing the effect of process k_j computed from a signal decomposition with a wavelet w and a filtering d. For the case of the hardness of contact wheel, Fig. 10 presents the evolutions of $F(R_q, w, d, \varepsilon)$ of the RMS parameters versus the scale for the decomposition of the details and all of the 8 wavelet shapes w.

In this paper only the effect of the stiffness of the wheel will be explained (the aim of this paper is to analyze only the effect of the wavelet shape on analysis; the physical meaning of the effects of all parameters was discussed in [22]). Fig. 10 shows that the contact wheel stiffness influences the amplitude at different scales. These results can be explained by the capacity of the contact wheel to transmit contact pressure to each grain of the belt. Indeed, the soft contact wheel is highly able to be deformed by the contact pressure to compensate grain size irregularities and surface topography. In this case, the pressure distribution on the belt surface is more uniform which induces a decrease in the local maximum pressure acting on the grains and, as a consequence, a lower penetration in tooled part decreases the roughness amplitude (Fig. 11).

At the microscopic scale, the stiffness effects on the mean width of the peaks are different. In fact, the soft contact wheel adapts its shape to cut the groove depths while for high stiffness, only the peak heights are in contact with the belt. As a result, the mean wavelength is shorter as seen in Fig. 12.

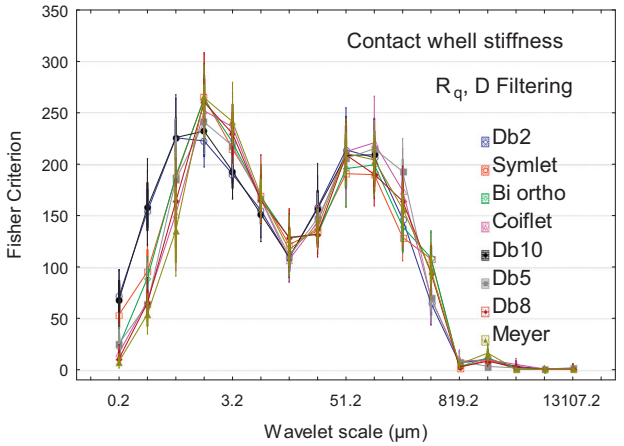

Fig. 10. Multiscale graph of relevance for the R_q roughness parameter computed with a D decomposition used to characterize the effect of contact wheel stiffness. The analysis is performed on the 8 retained wavelet forms.

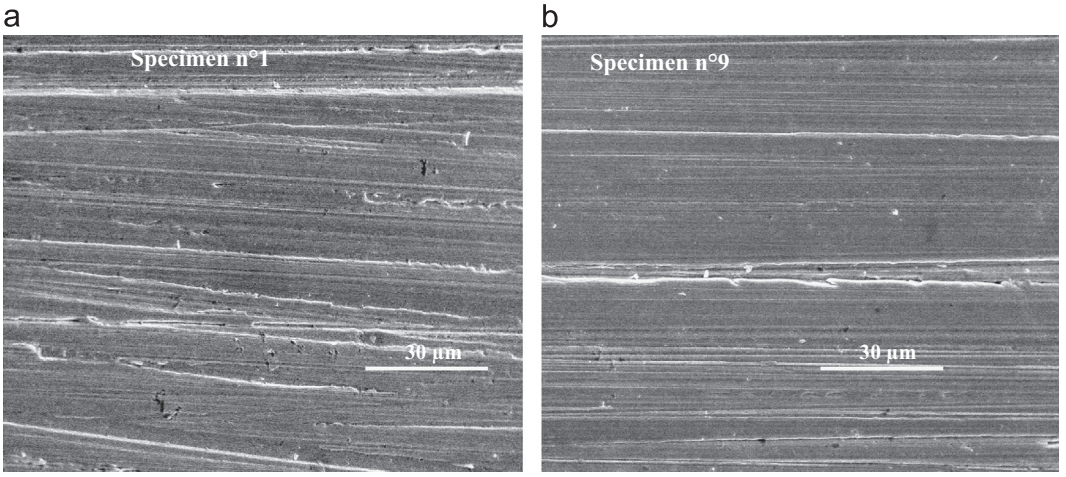

Fig. 11. SEM of specimens tooled with a hard contact wheel (on the left) and with a soft contact wheel (on the right) observed at a scale corresponding to the evaluation length of the fractal dimension [3].

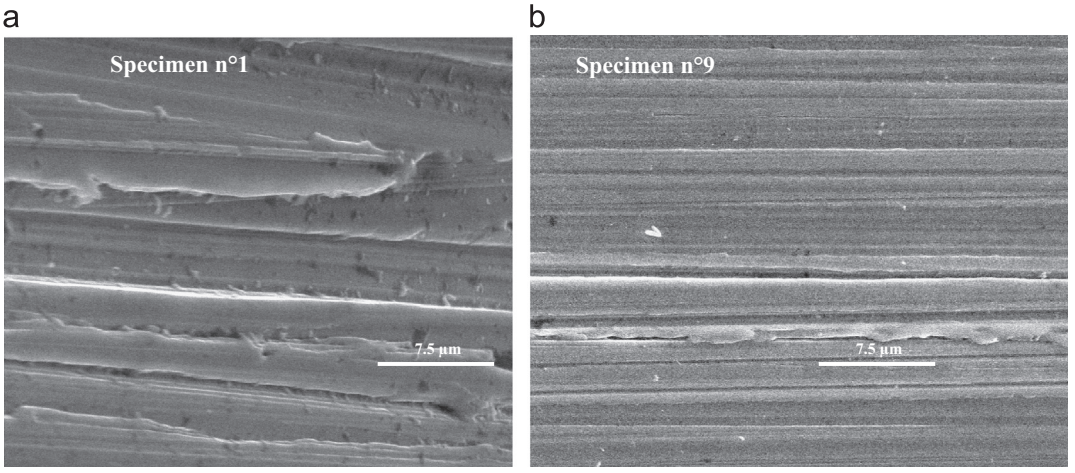

Fig. 12. SEM of specimens tooled with a hard contact wheel (on the left) and with a soft contact wheel (on the right) observed at the microscopic influence scale [3].

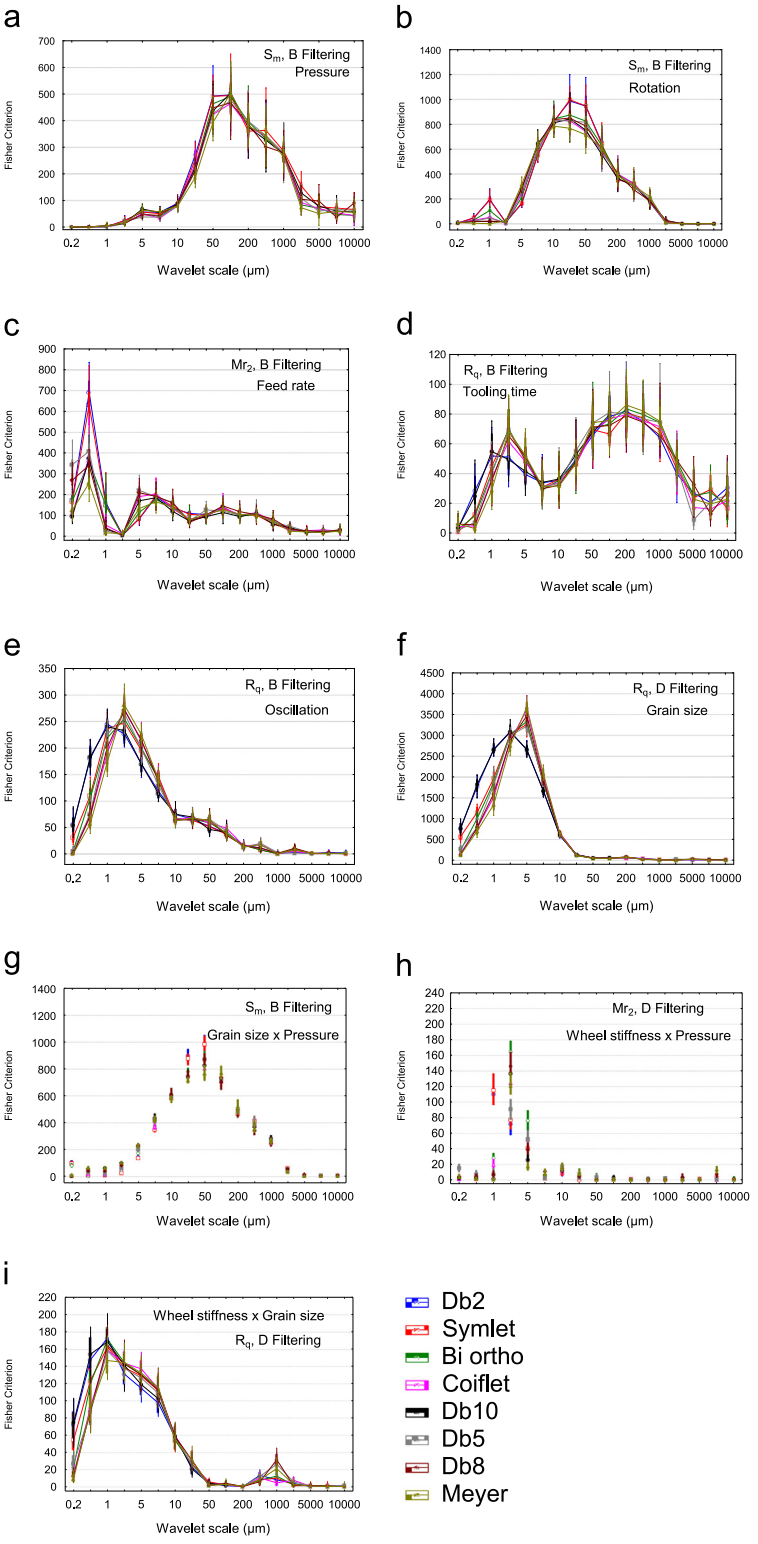

Fig. 13. Multiscale graphs of relevance for the more relevant roughness parameters computed with appropriate reconstruction used to characterize the effect of all process parameters and their associated interactions. This analysis is performed with the 8 retained wavelet forms.

Now for all process parameters and their associated interactions given by the experimental design, the pertinence graphs are plotted (Fig. 13).

6. Influence of the wavelet shape

The partial conclusion about the noninfluence of the wavelet shape in the above conclusion is not rigorously statistically proven. So far, it has been shown that at the maximal value of relevance, the confidence intervals do not allow to distinguish differences between wavelet shapes. Now a new analysis tool, based also on analysis of variance, is proposed to quantify the effect of the wavelet shape.

6.1. Multiscale relevance graph of wavelet shape

In this part, a new model of analysis of variance will be proposed. The basic idea is to avoid assumptions about a model between process parameters and roughness parameters. So, each of the 16 experiments will be considered as independent. The basic idea is to answer the following questions:

- Does a difference exist between roughness parameters computed at different scales and different filtering methods between the 16 experiments?
- Does the choice of wavelet shape influence globally the value of the roughness parameters for all experiments?
- Does the choice of the wavelet imply a noticeable difference way between the experiments?

To sum up these three questions into a unique one:

Does the shape of the wavelet influence the measure of relevance between the 16 experiments?

Towards this perspective, the following model of analysis of variance is proposed:

$$q_i(\varepsilon, d, w, e, n) = \alpha_0(i, d, \varepsilon) + \alpha_e(i, d, \varepsilon) + \alpha_w(i, d, \varepsilon) + \beta_{e,w}(i, d, \varepsilon) + \xi_{e,w,n}(i, d, \varepsilon) \tag{2}$$

where $q_i(\varepsilon, d, w, e, n)$ is the roughness parameter value of the n-th profile when the experimental design is taken at level e, for an ε scale decomposition with a filtering d computed with a wavelet w, $\alpha_0(i, d, \varepsilon)$ is the mean of $q_i(\varepsilon, d, w = \bullet, e = \bullet, n = \bullet)$, $\alpha_e(i, d, \varepsilon)$ is the influence on the roughness parameter value of the e-th experiment, $\alpha_w(i, d, \varepsilon)$ the effect of the wavelet independently of the experiments, and $\beta_{e,w}(i, d, \varepsilon)$ is the influence of the interaction between the e-th experiment and the wavelet shape w, and finally $\xi_{e,w,n}(i, d, \varepsilon)$ is a Gaussian noise with zero mean and σ standard deviation.

Fig. 15 represents the effect of relevance for the RMS roughness parameters (R_q). The following different remarks can be stated:

- The wavelet decomposition allows to locate the scale of relevance where experimental design reflects the topography. It means that, on the average, all process parameters intervene on a spatial scale around [0.2, 200 μm] and thus independently of the wavelet shape. The maximal relevance is around the size of the groove which means that the process parameters play a major role at the elementary scale of abrasion, i.e. taking account of the interaction *grain of the grit paper/steel* (tribological properties).
- The effect of a wavelet depends on the scale. At small scale < 4 μm, the F value is greater than unity meaning that the value of the R_q parameter differs with different wavelets. For the scale under 1 μm, the effect of wavelet becomes higher

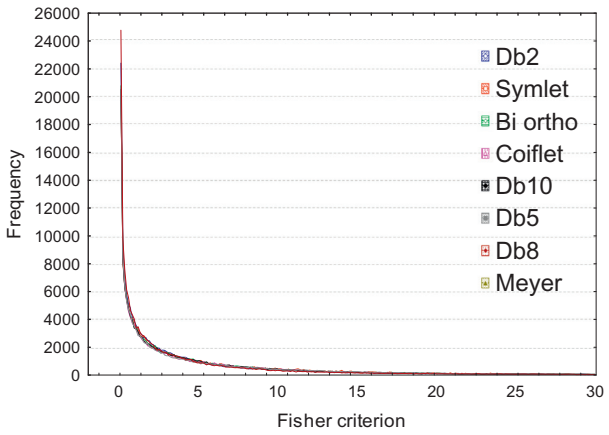

Fig. 14. Histogram of the F value when the computation of the roughness parameters is performed on the whole scanning length of the profile.

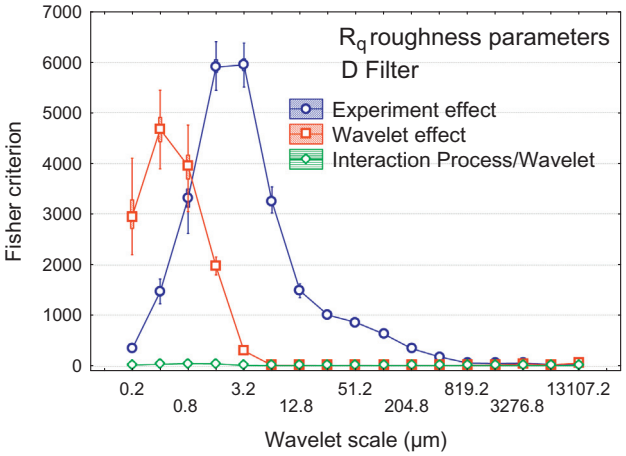

Fig. 15. Multiscale of relevance RMS roughness parameters (R_q).

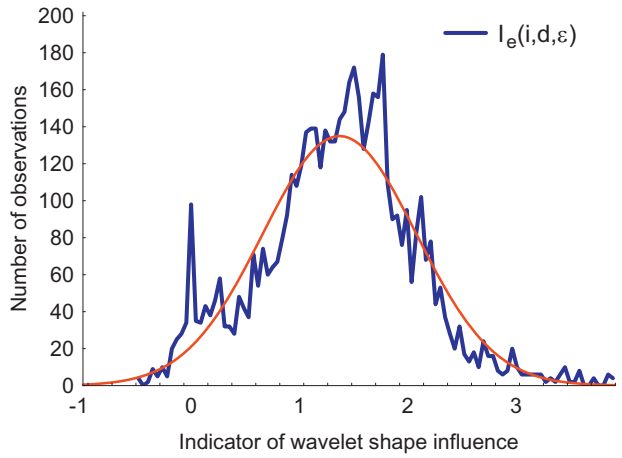

Fig. 16. Histogram of the indicator $I_e(i,d,\varepsilon)$ based on the Fisher criterion associated to the analysis of variance corresponding to all roughness parameters (see Table 2).

than the effect of the process parameters. At this small scale, the signal reconstruction is very robust in a statistical sense and then the morphology of wavelets is well quantified by the RMS (R_q) parameters. The graph of relevance of the *experiment effect* is not located on the same spatial scale as the *wavelet effect*. As a consequence, these relations cannot be linked to a possible bias of the proposed methodology.

- The interaction between *experiment effect* and *wavelet shape effect* is very low and can be neglected, for all the scales. This is a major result of our study: for the RMS parameters, the experimental effects are always the same whatever the wavelet shape.

6.2. Multiscale relevance indicator of the wavelet shape influence

In the previous section, it was shown that for the RMS parameters, the *experiment effect* is always the same whatever the wavelet shape. However, in our study, a hundred roughness parameters is computed. Then a global indicator must be built to quantify the effect of the wavelet including all filtering and all roughness parameters. Let us denote $F_e(i,d,\varepsilon)$ and $F_{e,w}(i,d,\varepsilon)$ as the Fisher criterion associated to the analysis of variance of the wavelet effect alone and wavelet and experiment interaction, respectively. The following indicator is then defined as

$$I_e(i,d,\varepsilon) = \log_{10}\frac{F_e(i,d,\varepsilon)}{F_{e,w}(i,d,\varepsilon)} \tag{3}$$

For $I_e(i,d,\varepsilon) > 0$, the effect of the plan is greater than that of the interaction, meaning that the relevance does not depend on the wavelet shape. Fig. 16 represents the histograms of the indicators. As it can be observed, the effect of the plan is higher

than the effect of the wavelet shape. As a consequence, the choice of wavelets does not affect the relevance of the effect of experiment. An analysis shows that the low values of $I_e(i,d,\varepsilon)$ are due to the fact that the concerned roughness parameters are not relevant and then $F_e(i,d,\varepsilon) \approx F_{e,w}(i,d,\varepsilon)$.

7. Discussion

The former analysis clearly demonstrates that the relevance does not depend on the wavelet shape: this assertion does not mean that a relevant roughness parameter is identical for a given profile reconstructed with any wavelet; the profile reconstruction does depend on the wavelet forms but a wavelet does not exist that better discriminates the morphology induced by the process of abrasion. However, wavelets are a powerful tool to locate the influence of the process parameters. There is an ambiguity: it was shown that the elementary process of abrasion is well defined by the Coiflet wavelet. However, this wavelet does not better characterize the effect of the process parameters than another wavelet that will fit the elementary process of abrasion (a scratch). This robust statistical analysis seems to defy the basic idea that an elementary wavelet shape plays a major role in detecting the scales of relevance in a complex signal. The signal of abraded surfaces is extremely complex due to multiscale effects with elevated variabilities. Even for the elementary scratch, the signal possesses a high deviance compared to an ideal shape. This deviance is due to an addition of microscopic influences (material heterogeneity, friction on interface, variation of loading, imperfect shape of the indentor, limitation in the surface reconstruction due to the curvature radius and the imperfect shape of the profilometer tip ….). All these structural variation introduce a high variation on the wavelet decomposition. Concerning the abraded surface, the tribological system is of course more complex. Basically, the abrasion can be seen as a succession of scratches but abrasive processes such as third body abrasion, strain hardening, wear of the grit, different sizes of the grit… lead to a high variation of this elementary model. All these interactions lead the abraded surfaces to possess a fractal structure. Then the spectrum presents a $1/f^{\alpha\alpha}$ structure with a high variance for a fixed frequency. This variation means that a wavelet at a given scale cannot precisely characterize the frequency response of the signal. An important result is that the signal reconstructed with a given wavelet at a given scale can be different from a signal obtained with another wavelet at the same scale. However, this difference does not depend on the process conditions. As a consequence, for the abraded surfaces, the choice of wavelet does not affect the conclusion about the multiscale analysis of abrasion. This important fact means that the relevance of the choice of the wavelet can only be performed by analyzing the capability to quantify disparities between two different signals and not the capability to reproduce finely the original signal.

8. Conclusion

It has been shown that the wavelet decomposition allows the quantification and the localization of the scales of abrasion for machining processes and thus for all process parameters. However, the relevance to characterize the appropriate scales of abrasion does not depend on the shape of the wavelet even if the Coiflet wavelet is appropriate to model the elementary process of abrasion (a single groove). Thanks to an original methodology of analysis of variance and bootstrap, the quantification of all effects is achieved for each process parameter and lead to the relevant signal indicator (roughness parameter). It is also shown that it is necessary to practice a multiscale analysis rather than a conventional one (analysis on all the scales of measure) to quantify all effects with accuracy.

From all the multiscale graphs of relevance, the following conclusions can be drawn:

- The methodology of relevance graph allows to quantify the spatial scale and the accurate filtering method to quantify the effect of process parameters and their associated interactions. In addition, this methodology allows also to distinguish different spatial stages. As can be observed in Fig. 13, bimodal curves appear for some process parameters (tooling time, wheel stiffness…). As a consequence, the physical origin of the morphological surface modification is certainly due to different mechanical interactions between the tool and the materials (mesoscopic interactions and macroscopic ones).
- At the scale of the measure (i.e. the scanning length of the surface, 8000 μm), it is difficult to find a relevant roughness parameter. To quantify this assertion, the empirical probability density function of the Fisher Criterion is plotted at the scale of the evaluation length (the whole signal) for all process parameters, all filterings, and all wavelets (Fig. 14). As can be observed, the relevance is very poor compared to the maximal Fisher Criterion computed at the appropriate scale. How to explain this fact? In fact, in roughness measurements, a difficult task is to find the reference from which roughness parameters will be computed. To have this reference, one must record the signal on a higher scale than the real spatial scale of the topographical phenomenon. The standard of roughness measurement imposes that the scanned surface is longer than five times the largest relevant wavelengths. This ratio of the whole scanned length defines a critical length. As a consequence, only the physical parameters under this critical length are meaningful. Then computing the roughness parameters at the evaluation scale leads to a poor discrimination. The multiscale analysis becomes a very powerful tool to obtain a relevant roughness characterization and the methodology that has been built, by analyzing the multiscale graphs of relevance allow to well visualize the power of the multiscale decomposition treatment compared to the usual treatment.

- The F Fisher criterion is always much greater than unity at the maximal scales of relevance for both appropriate roughness parameters and filtering method. This proves that all process parameters are relevant, i.e. influence the morphology of the surface. However, each process parameter does not get the same influence on the surface topography. Thanks to this methodology, a classification of the influence of the process parameters on surface topography can be done:

$$\begin{aligned}&\text{Grain size} \gg \text{Grain size}\\ &\times \text{pressure} > \text{rotation} > \text{wheelstiffness} = \text{feedrate} \gg \text{pressure} > \text{oscillation} > \text{Toolingtime} = \text{wheel stiffness}\\ &\times \text{ Grain size} \quad > \text{wheel stiffness} \times \text{pressure}\end{aligned}$$

- The use of the bootstrap due to the author's works [29,30] allows to give an uncertainty to the Fisher criterion. This knowledge of F confidence intervals allows quantification of the parameters that have statistically the same relevance. Moreover, this tool will be helpful to quantify the role of the wavelet shape in a final decision (Section 6).
- The wavelet shape does not affect the spatial localization of abrasion. As can be observed, the localization of relevance does not depend of the wavelet choice.
- Finally, whatever the shape of the wavelet, the relevance is the same whatever the level of relevance and thus for all the scales and all the process parameters. A point must be particularly emphasized that will be further explained and illustrated below: the relevance does not depend of the wavelets shape: this assertion does not mean that the relevant roughness parameter is the same for a given profile for all wavelets: profile reconstruction depends on the wavelet shape. However, a wavelet does not exist that better discriminates the morphology induced by the process of abrasion.

However, the reasons of the noninfluence of the wavelet shape on quantification of abrasion are still under discussion. A possible reason can be due to a high dispersion of the abrasion process that involves a complex signal that cannot be analyzed by the elementary shape of the wavelet. However, some investigations must be processed by simulating the process of abrasion with and without noise to validate this assumption.

Appendix A. Quantification of measurement errors due to tip radius curvature

Surface data of a fractal nature may be gathered in a very wide variety of ways. All involve a certain amount of smoothing or degradation of the true surface data according to the recording method. In laser profilometry, devices provide a smoothing measurement of the surface height via the interference patterns of the reflected height from a narrow beam [34]. With mechanical profilers, the stylus tip curvature radius incurs a smoothing effect on the surface and the information narrower than the stylus tip cannot be recorded. Since the smoothing effect is highly non-linear, it becomes very hard to estimate it on the original data [35,36]. The basic idea proposed here is to apply the theory of curvature radius to detect the scale on which the measurement system introduces a smoothing artefact on the measured data. In fact, the smoothing effect will increase the curvature radius on the scale measurement. It has been shown that the curvature radii of peaks of the surface can be analyzed by fractal analyses [37]. However, contrary to the previous ones, the method proposed by the authors allows the study of the surface roughness, by introducing a parameter, directly measured from the surface: the so-called, radius of asperity, defined as follows: $r_c = l_x^2/8l_y$ with $l_y = 0.1R_{\max}$or $l_y \approx 0.05R_{\max}$, and where $R_{\max}$is the maximal range amplitude of the profile. This method consists in finding the radius r_c of a circle of center O, passing by a crest A, and by two other points B and C of the profile; these two last ones being distant of l_x. The distances which separate the lines (B, C), respectively, from A and from O, are l_y and $r - l_y$ The parameter l_y is considered sufficiently small, so that the segment [A, O] is supposed to be perpendicular to [B, C], in its middle I. If we now apply Pythagoras' theorem to the triangle OBI, it then follows: $(l_x/2)^2 + (r_c - l_y)^2 = r_c^2$ Consequently, we get $r_c = (l_y/2) + (l_x^2/8l_y)$. By supposing l_y sufficiently small, and verifying

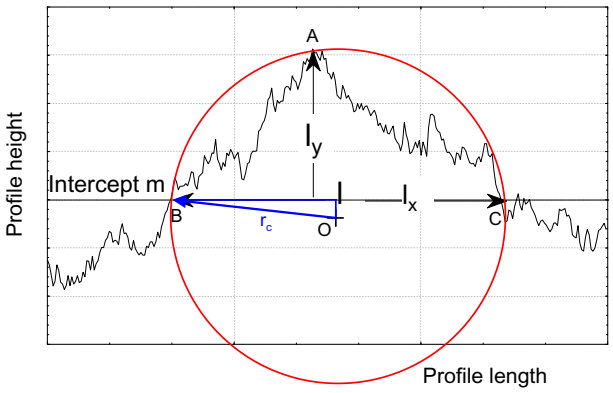

Fig. A1. Definition of l_x and l_y used to calculate the local curvature radius $r_c(l_x)$.

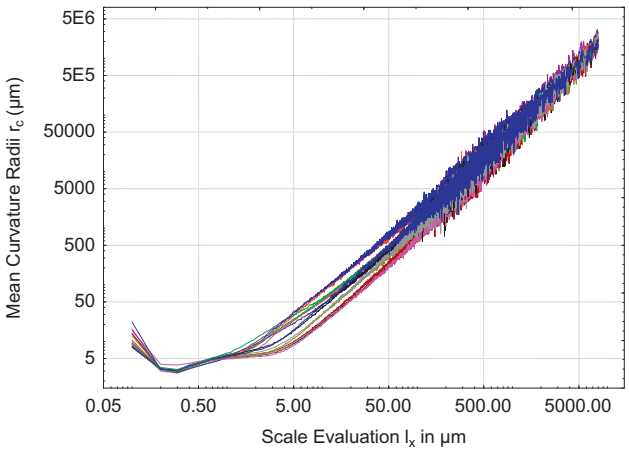

Fig. A2. Evolution of the mean curvature radius versus the observation scale for each tooled sample.

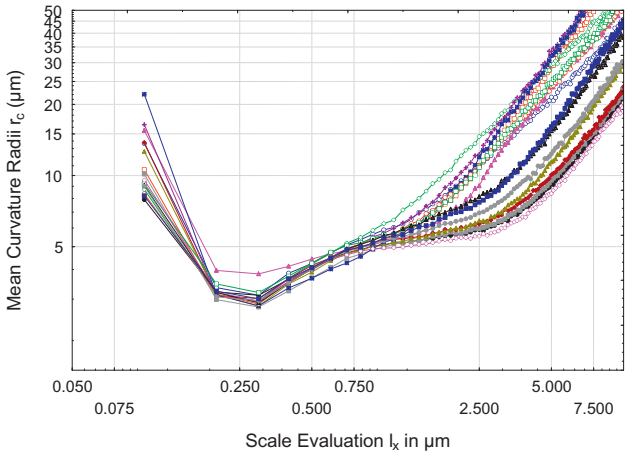

Fig. A3. Evolution of the mean curvature radius versus the observation scale for each tooled sample (zoom of Fig. A2.)

the following condition: $l_y < l_x$ then $r_c = (l_x^2/8l_y)$. Experimentally, the fractal dimension $\Delta(G_f)$ is obtained as a slope, by fitting in a log–log plot the discretized data $(\log l_x, \log r_c(l_x))$ where r_c is the curvature radii of peaks. r_c is obtained by an appropriate algorithm cutting the peaks randomly with a l_x width (Fig. A1). If the regression line fits well, the experimental data then allow writing:

$$r_c(l_x) = \alpha l_x^{\Delta(G_f)} \tag{A.1}$$

Fig. A2 represents these graphs for the sixteen measurements. As it could be shown on this last one, a cross over appears around 1 µm (Fig. A3). Below this threshold value, the different r_c estimations seem to be constant and over it, $r_c(l_x)$ follows the power law given by Eq. (A1). As a consequence, values less that 1 µm in the wavelet analyses must be used carefulness.

Appendix B. Comparison of various wavelet decompositions/choice of the relevant wavelet

The wavelet decomposition is applied on the individual scratch with the wavelet described below. The best local correlation is obtained for the Coiflet wavelet as it can be observed in Fig. B1. The values are centered on the scratch. The decomposition appears to be symmetric like the scratch morphology. Only DB2 presents a partial symmetry on its decomposition. All other wavelets have their maximal relevance not centered on the scratch. This seems to evidence a difficulty for other wavelets to localize the origin of the scratch. More drastically, for Meyer, DB8, Bior, DB10 two optima appear on left and right of the centre of the scratch. These wavelets will see two scratches rather than one and may be very poor theoretically to analyse the abrasion phenomenon.

Then an algorithm has been written to find the best value of the wavelet parameters that best fit the scratch. This is applied for all individual scratches (around 114 topographical measures of scratch corresponding to different locations and loads). Then the RMS of the residual between wavelet form and scratch morphology is computed. This RMS computation is

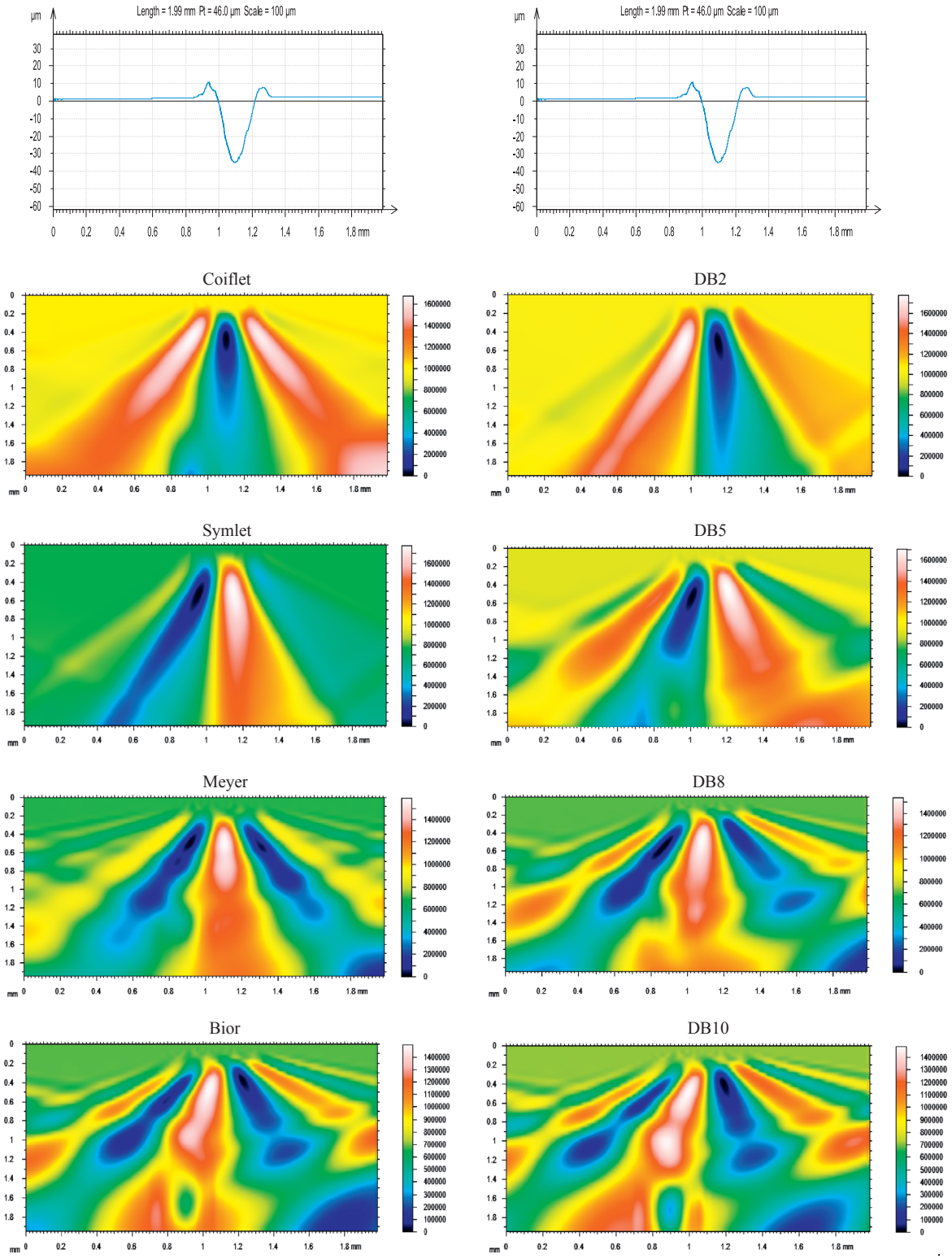

Fig. B1. Multiscale decomposition of the individual scratch (upper graphics) with different wavelet shapes retained in the analysis. The dotted line shows the position of the minimum value in the profile and is reproduced at the same position on each wavelet decomposition.

reproduced for the 114 measurements and descriptive statistics on RMS are evaluated. Fig. B2 represents the means of RMS with their associated standard errors. The best wavelet is Coiflet, with an error around 1 µm compared to 3 µm for others wavelets.

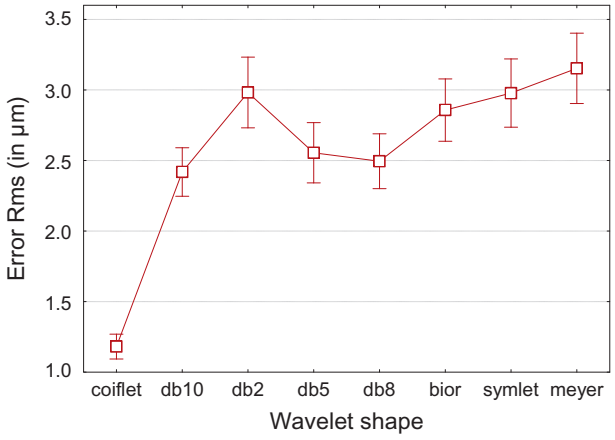

Fig. B2. Analysis of the root mean square error (in μm) of the residual between each wavelet and the scratch test signal.

References

[1] A. Khellouki, H. Maiz, J. Rech, H. Zahouani, Application de la méthode des plans d'expériences à la caractérisation du procédé de toilage de superfinition, in: Integrated Desing and Production, 4th International Conference, Casablanca, Maroc, November 2005.
[2] J. Rech, A. Moisan, Le toilage: un moyen d'optimisation de l'intégrité des surfaces usinées, 16ème Congrès Français de Mécanique, Nice, France, September 2003.
[3] D.V. de Pellegrin, G.W. Stachowiak, Evaluating the role of particle distribution and shape in two-body abrasion by statistical simulation, Tribology International 37 (2004) 255–270.
[4] M. Bigerelle, D. Najjar, A. Iost, Multiscale functional analysis of wear: a fractal model of the grinding process, Wear 258 (2005) 232–239.
[5] M. Bigerelle, A. Iost, A numerical method to calculate the Abbott parameters: a wear application, Tribology International 40 (2007) 1319–1334.
[6] M. Bigerelle, D. Najjar, A. Iost, Mechanical modeling of micro-scale abrasion in superfinish belt grinding, Tribology International 41 (2008) 992–1001.
[7] V. Gorana, V. Jain, G. La, Prediction of surface roughness during abrasive flow machining, International Journal of Advanced Manufacturing Technology 31 (2006) 258–267.
[8] T.G. Mathia, M. Ouadou, V. Jardret, Fully computerised sclero-topometer, in: Commission of the European Communities, Ch. Velzel, L. Baker Philips Eindhoven (Eds.), Proceedings of EU Measurement and Testing Workshop – Surface Characterization and Microhardness Measurement, 1994.
[9] R.J. King, D.E. Putland, S.P. Talim, The abrasion of optical coatings and its assessment, Journal of Physics E: Scientific Instruments 21 (1988) 39–46.
[10] T.K. Puthanangady, S. Malkin, Experimental investigation of the superfinishing process, Wear 185 (1995) 173–182.
[11] B. Varghese, S. Malkin, Experimental investigation of methods to enhance stock removal for superfinishing, Annals CIRP 47 (1995) 231–234.
[12] S.H. Chang, T.N. Farris, S. Chandrasekarc, Experimental analysis on evolution of superfinished surface texture, Journal of Materials Processing Technology 203 (2008) 365–371.
[13] J.A. Randi, J.C. Lambropoulos, S.D. Jacobs, Subsurface damage in some single crystalline optical materials, Applied Optics 44 (2005) 2241–2249.
[14] P.P. Hed, D.F. Edwards, Optical glass fabrication technology: relationship between surface roughness and subsurface damage, Applied Optics 26 (1997) 4677–4680.
[15] P.E. Miller, T.I. Suratwala, L.L. Wong, M.D. Feit, J.A. Menapace, P.J. Davis, R.A. Steele, The distribution of subsurface damage in fused silica, Proceedings of the SPIE 5991 (2005) 1–25.
[16] S. Jha, V.K. Jain, Modeling and simulation of surface roughness in magnetorheological abrasive flow finishing (MRAFF) process, Wear 261 (2006) 856–866.
[17] P. Podsiadlo, G.W. Stachowiak, Fractal-wavelet based classification of tribological surfaces, Wear 254 (2003) 1189–1198.
[18] C.Q. Yuan, J. Li, X.P Yan, Z. Peng, The use of the fractal description to characterize engineering surfaces and wear particles, Wear 255 (2003) 315–326.
[19] G. Shirong, C. Gouan, Fractal prediction models of sliding wear during the running-in process, Wear 231 (1999) 249–255.
[20] B. Bhushan, A. Majumdar, Elastic-plastic contact model for bifractal surfaces, Wear 153 (1992) 53–64.
[21] J.J. Wu, Characterization of fractal surfaces, Wear 239 (2000) 36–47.
[22] A. Van Gorp, M. Bigerelle, M. El Mansori, P. Ghidossi, A. Iost, Effects of working parameters on the surface roughness in belt finishing process: the size-scale estimation influence, International Journal of Materials and Product Technology 38 (1) (2010) 16–34.
[23] K. Hokkirigawa, K. Kato, Z.Z. Li, The effect of hardness on the transition of the abrasive wear mechanism of steels, Wear 123 (2) (1988) 241–251.
[24] V. Jardret, H. Zahouani, J.L. Loubet, TG. Mathia, Understanding and quantification of elastic and plastic deformation during a scratch tests, Wear 218 (1998) 8–14.
[25] A.A. Torrance, The influence of surface deformation on mechanical wear original research, wear 200 (1996) 45–54.
[26] J.L. Bucaille, E. Felder, G. Hochstetter, Mechanical analysis of the scratch test on elastic and perfectly plastic materials with the three-dimensional finite element modeling, Wear 249 (2001) 422–432.
[27] T.G. Mathia, L.B. Sclerometric, Characterization of nearly brittle materials, Wear 198 (1986) 385–399.
[28] M. Bigerelle, B. Hagege, M. El Mansori, Modelisation of abrasion: application on superfinishing by belt grinding process, Tribology International 41 (11) (2008) 992–1001.
[29] M. Bigerelle, P. Rocher, H.F. Hildebrand, A. Iost, A new polishing process of dental alloys, Journal of Dental Research 80 (4) (2001) 1206.
[30] M. Bigerelle, T. Mathia, S. Bouvier, The multi-scale roughness analyses and modeling of abrasion with the grit size effect on ground surfaces, Wear 286 (2012) 124–135.
[31] A. Petropulu, Detection of transients using discrete wavelet transform, in: ICASSP-92: International Conference on Acoustics, Speech, and Signal Processing, vol. 2, 1992, pp. 477–480.
[32] A. Abbate, J. Koay, J. Frankel, S.C. Schroeder, P. Das, Application of wavelet transform signal processor to ultrasound, in: Proceedings of the 1994 Ultrasonic Symposium, 94CH3468-6, 1994, pp. 1147–1152.
[33] P. Rizzo, F. Lanza di Scalea, Discrete wavelet transform to improve guided-wave-based health monitoring of tendons and cables, in: Conference on Smart Structures and Materials, Proceedings of SPIE, vol. 5391, 2004, p. 523.

[34] C.Y. Poon, B. Bhushan, Comparison of surface roughness measurements by stylus profiler, AFM, and non-contact optical profiler, Wear 190 (1995) 76–88.
[35] V. Radhakrishnan, Effect of stylus radius on the roughness values measured with tracing stylus instruments, Wear 16 (1970) 325–335.
[36] D.J. Whitehouse, Theoretical analysis of stylus integration, Annals CIRP 23 (1974) 181–182.
[37] M. Bigerelle, J.M. Nianga, D. Najjar D, A. Iost, C. Hubert, K.J. Kubiak, Roughness signature of tribological contact calculated by a new method of peaks curvature radius estimation on fractal surfaces, Tribology International (2013). (in press).
[38] F. Maurizio, C. Lorenzo, Composite continuous wavelet transform of potential fields with different choices of analyzing wavelets, Journal of Geophysical Reasearch – Solid Earth 116 (2011) B07104.
[39] S. Mezghani, L. Sabri, M. El Mansori, H. Zahouani, On the optimal choice of wavelet function for multiscale honed surface characterization, Journal of Physics Conference Series 311 (2011) 012025.
[40] L. Cherif, S.M. Hamza, M. Debbal, F. Bereksi-Reguig, Choice of the wavelet analyzing in the phonocardiogram signal analysis using the discrete and the packet wavelet transform, Expert Systems with Applications 37 (2010) 913–918.
[41] K. Darowicki, A. Zielinski, Optimal wavelet choice in electrochemical experiments, Fluctuation and Noise Letters 6 (2006) 215–225.
[42] N. Ahuja, S. Lertrattanapanich, N.K. Bose, Properties determining choice of mother wavelet, IEEE Proceedings – Vision Image and Signal Processing 152 (2005) 659–664.
[43] N. Guan, K. Yashiro, S. Ohkawa, On a choice of wavelet bases in the wavelet transform approach, IEEE Transactions on Antennas and Propagation 48 (2000) 1186–1191.
[44] A.H. Tewfik, D. Sinha, A.P. Jorgensen, On the optimal choice of a wavelet for signal representation, IEEE Transactions on Information Theory 38 (1992) 747–765.